Sliding induced adhesion of stiff polymer microfiber arrays:

1. Macroscale behaviour

By Jongho Lee[1]†, Carmel Majidi[2], Bryan Schubert[2], Ronald S. Fearing[2]

[1] *Department of Mechanical Engineering*

[2] *Department of Electrical Engineering & Computer Sciences*

University of California

Berkeley, CA 94720, USA

Gecko-inspired micro fiber arrays with 42 million polypropylene fibers per square centimetre (each fiber with elastic modulus 1 GPa, length 20 micrometres and diameter 0.6 micrometre) were fabricated and tested under pure shear loading conditions, after removing a preload of less than 0.1 N per square centimetre. After sliding to engage fibers, 2 square centimetre patches developed up to 4 newtons of shear force with an estimated contact region of 0.44 square centimetres. The control unfibrillated surface had no measurable shear force. For comparison, a natural setal patch tested under the same conditions on smooth glass showed about 7 times greater shear per unit estimated contact region. Similar to gecko fiber arrays, the synthetic

† To whom correspondence should be addressed. E-mail: jongho@eecs.berkeley.edu

patch maintains contact and increases shear force with sliding. The high shear force observed (approximately 210 nN per fiber) suggests that fibers are in side contact, providing a larger true contact area than would be obtained by tip contact. Shear force increased over the course of repeated tests for synthetic patches, suggesting deformation of fibers into more favorable conformations.

Keywords: bio-inspired adhesion, gecko, friction, shear, sliding

1. Introduction

Natural geckos have exceptional wall-climbing ability using their millions of micro/nano fibrillar structures. The gecko's keratin fiber arrays form a unique attachment mechanism which is non-adhesive by default (Autumn & Hansen 2006c), but can be easily engaged with low compressive preload and sliding to develop high shear force (Autumn *et al.* 2000), and controllably released with low pull-off force (Gravish *et al.* 2007). These properties of natural gecko are critical for efficiently and reliably running up walls. In characterizing the behaviour of a "directional" adhesive, we refer to the tensile force (normal to a surface) and the shear force (parallel to a surface). It is important to note that the tensile and shear force can be strongly coupled, and may depend on both compressive preload (normal to surface) and engagement trajectories. In this paper, we examine the macro-scale behaviour of a synthetic gecko patch. As the whole patch is non-adhesive by default in the normal direction, the patch is tested under pure shear loading, where forces

are constrained to be parallel to a surface.† Under shear loading, membrane buckling effects dominate behaviour. In part II of this paper, Schubert *et al.* (2007b) examines a micro-scale spherical indentation of a synthetic gecko patch which is fixed to a backing layer to avoid membrane buckling effects. Under combined shear and normal loading the patch demonstrates a *frictional adhesion* effect, whereby a normal tensile load can be supported only under conditions of an applied shear load.

There is increasing interest by researchers in understanding and fabricating Gecko-inspired Synthetic Adhesives (GSAs) (Autumn 2007, Autumn & Gravish 2007) using materials which range in hardness from soft polymers to carbon nanotubes ($E \sim 3\times10^5$ to 10^{12} Pa). Harder materials allow greater fiber packing density (Sitti & Fearing 2003), and likely better resist wear and particle contamination. Recent work using soft polymer fiber arrays (Kim & Sitti 2006, Santos *et al.* 2007, Gorb *et al.* 2006) has increased normal adhesion several times over the bulk material. Multiwalled carbon nanotubes (MWCNT) (Zhao *et al.* 2006, Ge *et al.* 2007) and low-aspect-ratio (length/diameter = 0.5 to 10) hard polymer stalks (Geim *et al.* 2003) demonstrated tensile adhesion but they require high normal compressive preload. Kustandi *et al.* (2007) has recently demonstrated 0.7 N/cm^2 tensile adhesion with preload pressure of 1 N/cm^2 using 10:1 aspect ratio hard polymer fibers ($E \sim 2.8$ GPa).

Fiber arrays have also demonstrated high friction forces (that is, high shear forces with normal compressive loads which engage fibers) such as Majidi *et al.*

† Pure shear loading with zero normal load or peeling moment was also used by Ge *et al.* (2007) and Zhao *et al.* (2006) to test patch behaviour, and is well known in materials testing, e.g. (Antoniou & Bastawros 2003).

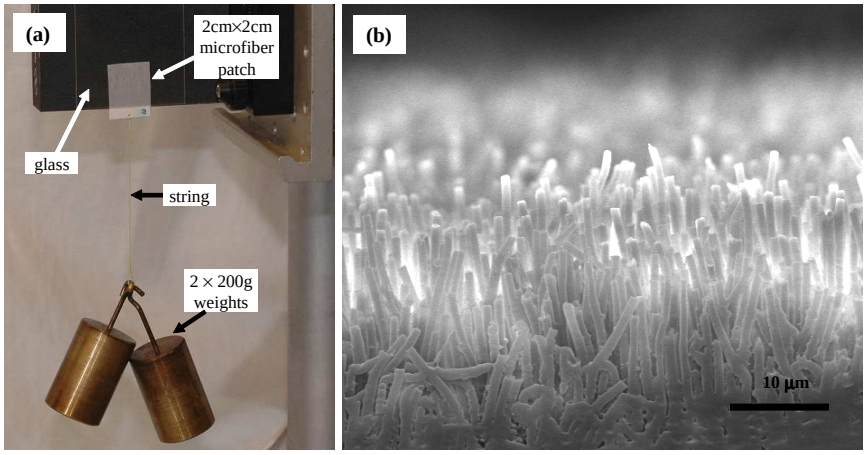

Figure 1. (a) A 2 cm × 2 cm microfiber array patch holding two 200 gram weights (400 gram) on a vertical smooth glass slide without normal load. (b) Scanning electron microscope(SEM) image of a microfiber array.

(2006) with coefficient of friction $\mu > 5$ using polypropylene and Aksak *et al.* (2007b) with $\mu > 1$ using MWCNT. The shear force required a sustained normal compressive load and the samples did not show shear or tensile adhesion.

To simultaneously obtain high shear force and low tensile pull-off forces with a low initial compressive preload, we have designed an array of microfibers which makes side contact with a surface (Majidi *et al.* 2005). In contrast, structures such as Geim *et al.* (2003) and Kustandi *et al.* (2007) use tip contact of fibers. We fabricated an array of 0.6 μm diameter polypropylene fibers whose elastic modulus (E $\sim$ 1 GPa) and aspect-ratio ($\sim$ 30), are similar to natural tokay gecko setae with E $\sim$ 1.5 GPa (Peattie *et al.* 2007, Autumn *et al.* 2006a) and aspect-ratio $\sim$ 25 (Ruibal & Ernst 1965). In contrast to Majidi *et al.* (2006), these patches were fabricated with reduced backing curvature to enable fiber engagement without sustained compressive normal loading. (The important effect of backing curvature

on adhesion is discussed in Schubert *et al.* (2007a).) The flat backing samples with millions of microfibers shows shear adhesion as demonstrated in figure 1.

In this paper, we first directly compare the stiff polymer based microfiber adhesive to a natural gecko setal array under pure shear loading. The high elastic modulus material and vertical fibers make the fiber array intrinsically non-adhesive by default. (Angled fibers as suggested by Sitti & Fearing (2003) could be used to have an initially adhesive state.) We show experimentally that high shear adhesion can be induced by sliding displacement alone with minimal initial normal compressive preload, but can be easily detached in the normal tensile direction (low 90^o peel strength). We also show that the adhesion demonstrated in figure 1 does not depend on an internal viscoelastic property. Durability of some previous GSAs has been a problem, e.g. Zhao *et al.* (2006). Tests of the polypropylene (PP) microfiber array showed an increase in shear adhesion force with repeated uses. In the Discussion, we demonstrate that the measured shear stress in the estimated contact region of 9 N/cm^2 is consistent with fibers in side contact with the surface.

2. Material and Methods

(*a*) *Material preparation*

GSA samples were fabricated by casting a single layer of 25 μm thick polypropylene (TF-225-4, Premier Lab Supply Inc.) in a vacuum oven at $200°C$ into a 20 μm thick polycarbonate filter (ISOPORE, Millipore Inc.) containing 0.6 μm diameter pores. The polycarbonate filter was etched in methylene chloride, and resulting samples were rinsed in iso-propyl alcohol and air dried. Backing curvature was significantly reduced compared to previous microfiber arrays (Majidi *et al.* 2006),

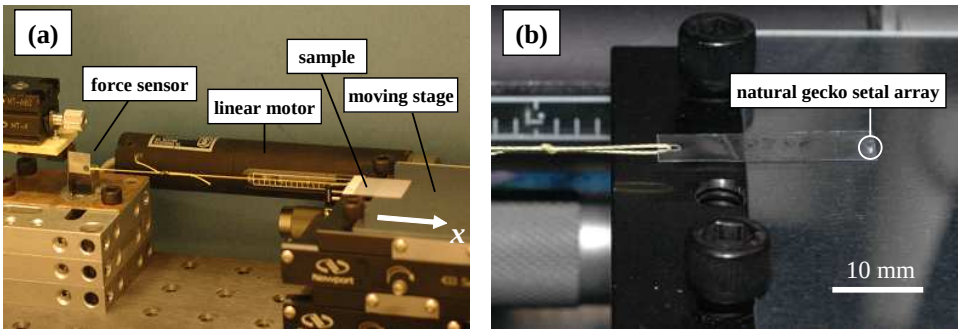

Figure 2. (a) Testing setup : shear force of a 2 cm × 2 cm synthetic microfiber array patch on a glass slide is being measured while the stage is driven in the x-direction by the linear motor. (b) Natural gecko setal array under shear load on same test setup.

increasing the number of fibers in contact and adhesion. Using a fixed fiber length, the fiber diameter was selected to provide enough compliance while preventing fibers from clumping. Control measurements were performed on processed 25 μm thick polypropylene film that underwent the same fabrication steps as the fiber arrays, with the exception that no polycarbonate filter was applied. Both the microstructured samples and controls were cut into 2 cm × 2 cm squares. For some samples which demonstrated higher shear force than the limit of the force sensor, smaller areas (2 cm × 1.2 cm and 2 cm × 0.8 cm) were used.

Natural gecko setal arrays were prepared by N. Gravish, M. Wilkinson and K. Autumn in the Department of Biology, Lewis and Clark College, Portland, OR, USA. Individual lamellae were isolated from tokay geckos. Each isolated lamella was fixed to the end of a 2.5 cm × 0.6 cm × 0.02 cm acetate strip using cyanoacrylate SuperGlue Gel. The areas of gecko setal arrays tested were 0.11 cm × 0.03 cm and 0.18 cm × 0.03 cm.

(*b*) *Measurement methods*

Macro-scale shear adhesion tests during sliding with no normal compressive load were performed with the single axis force sensor system in figure 2(a). The system is composed of a stepper motor (TS Products model 2200) driven linear stage with a linear variable differential transformer (LVDT) position sensor (MEPTS-9000, Techkor Instrumentation), and double cantilever force sensor (Schubert *et al.* (2007a)). The force sensors were calibrated with known weights. The force sensor for microfiber array samples had stiffness 10^5 N/m and resolution < 42 mN. A more sensitive force sensor (stiffness 3×10^4 N/m, resolution < 13 mN) was used for natural gecko setal arrays.

Each sample was connected to a force sensor using a string (Kevlar, Dupont) and was placed on a glass slide (Microscopes slides, Fisher Scientific) on top of the stage. The glass slide had surface roughness (root mean square(RMS) = 3.3 nm, see supplement material) and was cleaned using isopropanol to remove dust before using. Before shear testing, a normal preload pressure (< 0.1 N/cm^2) was applied by gloved finger to remove any possible initial curvature of the backing. A separate test showed that the preload used had a negligible effect on shear force. After the preload was removed, the stage was driven at constant speeds which ranged from 48 to 240 μm/s in the x-direction in figure 2(a). During testing, the normal stress due to weight of the patch was less than 0.3 mN/cm^2. This normal stress is not needed to sustain shear stress as can be seen in figure 1(a). The gecko setal array under testing is shown in figure 2(b). While driving the stage, shear force and stage displacement were recorded by a 4 channel digital oscilloscope (TDS3014B, Tektronix).

Estimated contact region of samples was recorded by a camcorder (DCR-TRV520, Sony) using reflected white light through the back of the sample. This estimated contact region represents regions where fibers may be touching the glass substrate. Due to backing membrane roughness, all fibers in the bright region are not necessarily touching the glass.

3. Results

For both the microfiber array and natural gecko, shear force increased with sliding distance. The microfiber sample continued to function after 50 pure shear tests. In addition to durability, repeated sliding tests showed increase of maximum shear force of microfiber array samples.

As plotted in figure 3, shear force during sliding of a 2 cm $\times$ 2 cm microfiber patch increased as the patch was pulled on a smooth glass slide in the tangential (x) direction with no normal load. (Pressure due to weight of patch < 0.3 mN/cm^2.) Pulling velocity for the stage was 120 μm/s. Effects of other preloads and velocities are presented later in this paper. Initially, shear force increased as the stage moved for the first several millimetres and saturated at approximately 4 N shear force. From examination of captured images, the sample did not slide until the shear force exceeded 1 N. Images 1-6 in figure 3 show that estimated contact region (white amorphous regions) on glass increases as the synthetic microfiber patch slides. In image 1, the square patch placed on a glass slide had just several tiny contacting points after normal preload was removed. As the glass moved to the right (image 2-6), the initial contact areas grew. Even though the sample lost some overall overlap area (white square region in images 4-6) with the glass because the glass slid to the

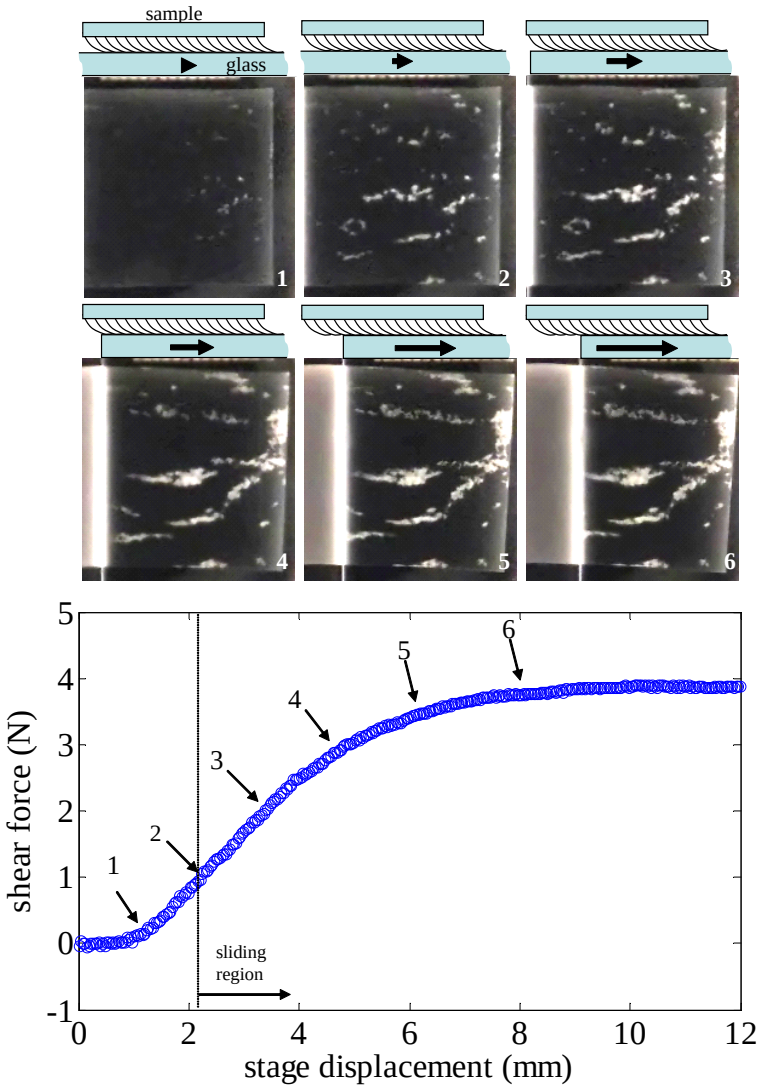

Figure 3. Shear force of a 2 cm × 2 cm synthetic microfiber array with zero normal load increased monotonically during tangential displacement (stage velocity $V_x = 120$ μm/s). Top images : Estimated contact region (white amorphous regions) at indicated times. Shear force increases even as patch slides off glass. Estimated contact region is 11% of patch area, with possible buckling of membrane in dark (non-contact) regions.

right, absolute shear force increased. The peak shear stress with estimated contact area fraction (white amorphous area (0.44 cm^2) / patch area (4 cm^2)) of 11% was 9 N/cm^2. The white amorphous estimated contact region was determined by image processing (MATLAB R2006a, The MathWorks Inc.). The control (RMS surface roughness 6.8 nm, see supplement material), unstructured polypropylene, had no observable shear stress (< 0.3 mN/cm^2). The microfiber arrays have high shear adhesion but low normal adhesion. For example, only 3 ± 0.4 mN (mean$\pm$s.d., N = 5) of perpendicular force is required to peel the sample from glass. This corresponds to a 90^o peel strength of 0.15 ± 0.02 N/m.

Tests with a 0.18 cm $\times$ 0.03 cm natural gecko setal array with a gravitational compressive normal stress (< 50 mN/cm^2) showed similar sliding induced shear force and saturation (see figure 4). No external preload was applied. Pulling velocity for the natural gecko setal array was 120 μm/s. The top images in figure 4 show relative position of the natural setal array and glass under testing at indicated times. The images indicate that the gecko setal array started sliding after the shear force exceeded 0.2 N, and shear force approximately saturated after 200 μm displacement. Because of an initially slack string, stiffness of the force sensor system including a string is nonlinear. Linearized stiffness of the system is 250 N/m for 0 N $\sim$ 0.2 N and 1600 N/m for 0.2 N $\sim$ 1.6 N. Because of this low stiffness (250 N/m) for low load (< 0.2 N), the gecko setal array did not slide until after 960 μm of stage movement, corresponding to 0.24 N shear force.

Velocity dependence was examined for both the synthetic adhesive and natural gecko setal array. Both samples were pulled four times at each velocity from 48 μm/s to 240 μm/s. Average and standard deviation of plateau force are plotted

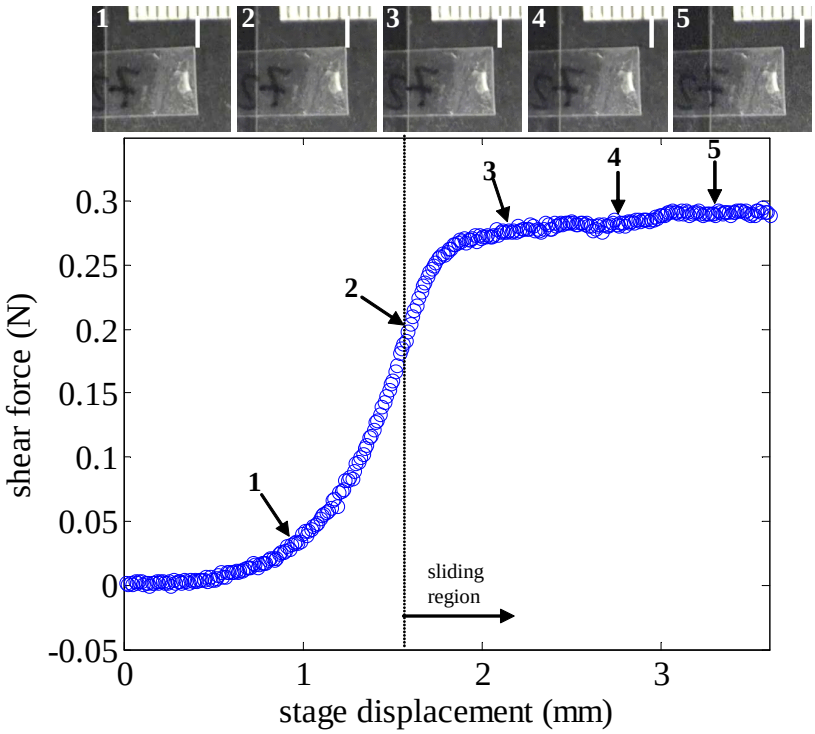

Figure 4. Shear force of a 0.18 cm × 0.03 cm natural gecko setal array with zero normal load during tangential displacement of the stage (stage velocity $V_x = 120$ μm/s). Top images : natural setal array under testing at indicated times. The captured images indicate that the sample actually began sliding at 13 sec due to compliance of the sensor system including the string.

in figure 5. No drastic change in shear force with velocity was seen for microfiber arrays or the natural gecko setal array.

In many GSAs, e.g. Gorb *et al.* (2006) and Kim & Sitti (2006) tensile adhesion force is a strong function of normal preload. Before shear testing, an approximately uniform preload was applied, and carefully removed before testing without disturbing the patch. A sheet of polydimethylsiloxane (PDMS) was used to distribute normal loading uniformly over a sample. A cloth (Technicloth, ITW Techwipe Inc)

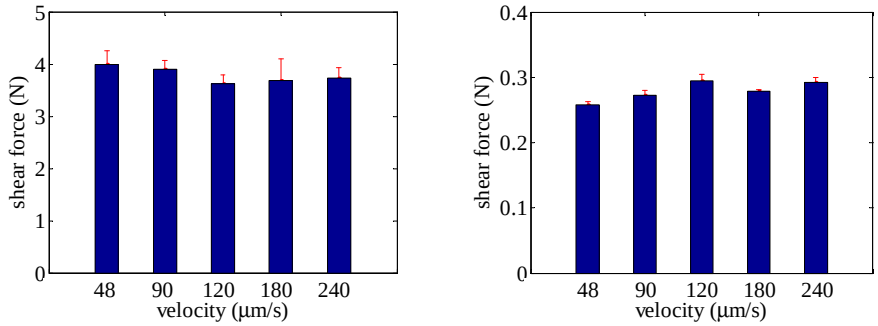

(a) Synthetic microfiber array. (b) Natural gecko setal array.

Figure 5. Maximum shear force for various velocities. Each sample was tested 4 times at each velocity. Patch sizes of the synthetic microfiber array and natural gecko setal array are 2 cm × 0.8 cm and 0.18 cm × 0.03 cm respectively.

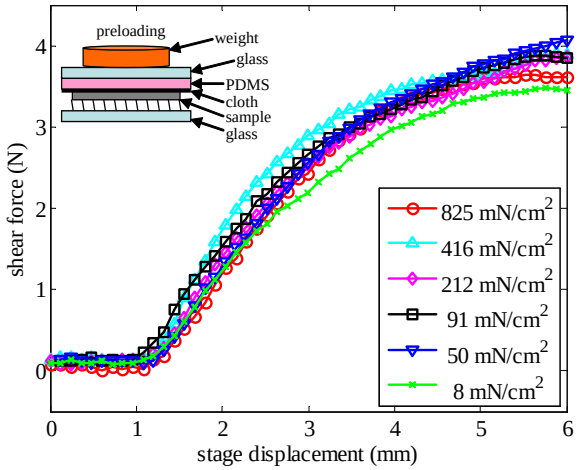

Figure 6. Shear force of a 2 cm × 1.2 cm microfiber array with different preloads. The sample was preloaded uniformly using a cloth, PDMS, glass and a weight.

prevented soft PDMS sticking to a sample. After carefully removing the stack on a microfiber array patch, the patch was pulled at 120 μm/s. Figure 6 shows sliding induced shear adhesion for different preloads (8 mN/cm^2 $\sim$ 825 mN/cm^2), with

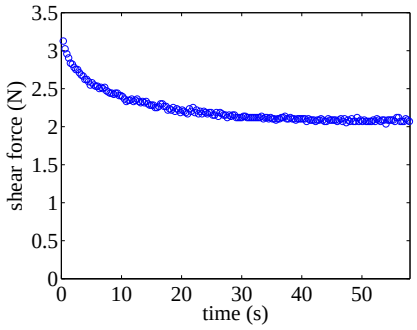

(a) Synthetic microfiber array.

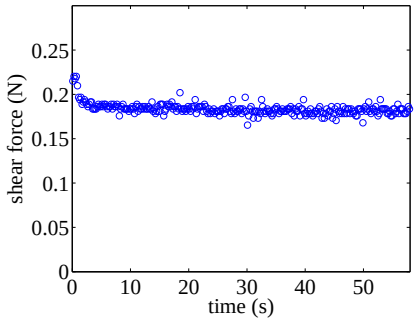

(b) Natural gecko setal array.

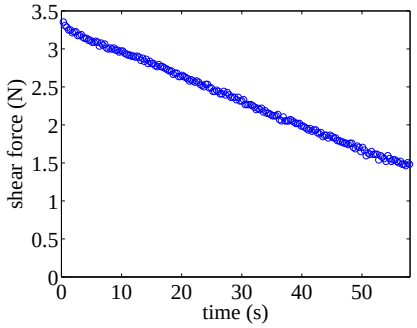

(c) Pressure sensitive adhesive.

Figure 7. Comparison of relaxation behaviour of a microfiber array, natural gecko setal array and PSA after the stage stopped moving. Shear force of a microfiber array and natural gecko setal array decreased about 30% and 20% respectively and maintained constant level, while the PSA kept losing its shear force.

no observable relation between preload and maximum shear force. In other tests, the microfiber array samples were gently preloaded (< 0.1 N/cm^2) with a gloved forefinger for simplicity, since preload did not significantly affect maximum shear force.

Relaxation behaviour of PP microfiber arrays and the gecko setal array was

significantly less than pressure sensitive adhesives (PSAs) (Magic tape, Scotch®, 3M) whose adhesion relies heavily on internal viscous conformation. After engaging the array by sliding, the moving stage stopped at time 0 and shear force relaxation is plotted in figure 3 for a synthetic microfiber array and in figure 3 for a natural gecko setal array. After stopping, the microfiber array patch crept about 150 μm without leaving residue on the glass slide. Consequently, the shear force of the microfiber array decreased by 30% and then maintained a constant shear force. This experiment supports that shear adhesion of the synthetic patch does not depend on viscoelasticity of the material but sliding of microfibers on glass (see Discussion). After stopping, as with the microfiber array, shear force of the natural gecko setal array also decreased by 20%, then maintained a constant level. In contrast to a microfiber array and natural gecko setal array, a 0.2 cm $\times$ 0.5 cm PSA adhered and did not slide on glass during loading. After stopping the stage at 0 sec, the PSA crept while leaving much soft polymer residue on the glass. Consequently, shear force kept decreasing as shown in figure 3.

Microfiber array patches survived more than 50 high shear tests without a reduction in shear force. Instead of a reduction in force, a training effect was observed with repeated tests. As the sample was dragged repeatedly with zero normal load, maximum saturated shear force increased as shown in figure 8.

When shear force approached saturation, the sample sometimes slipped, presumably due to buckling of the thin backing of the patch as shown in the fifth test in figure 8. Shear force drops were also observed with natural gecko setal arrays at high load. For both materials, shear force recovered after slip events.

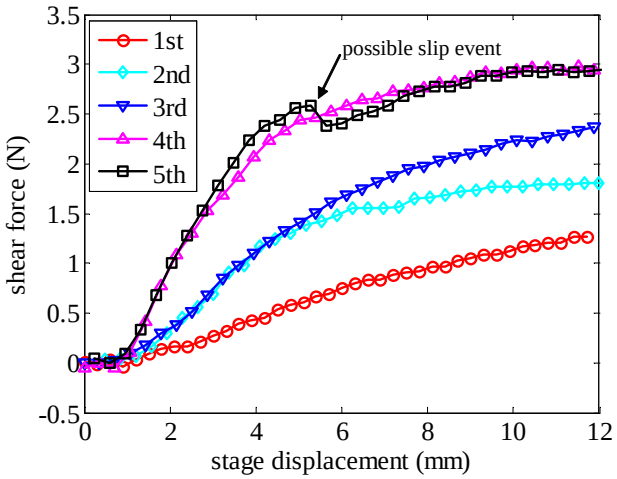

Figure 8. Shear force of a 2 cm × 2 cm microfiber array with repeated trials at 5 minute intervals after the array had relaxed for 4 days. For the sample, $V_x = 120$ μm/s.

4. Discussion

Experimental results with centimetre-size microfiber arrays have shown several key GSA properties, including relatively strong shear adhesion with low peel strength, low normal preload for fiber engagement, and durability over multiple attachment cycles. We discuss using a fiber side-contact model to explain the observed shear forces. Angling of the fibers after sliding can be observed in microscope images, and is consistent with the increase in shear adhesion with use. Finally, we compare the performance of various GSAs, and discuss how the behaviour of the polypropylene microfiber array relates to tasks such as wall-climbing.

(*a*) *Shear adhesion induced side contact*

The shear stress shown in figure 3 saturates at approximately 9 N/cm^2 per unit estimated contact region. With a fiber density of $\rho = 42 \times 10^6$ fibers per square

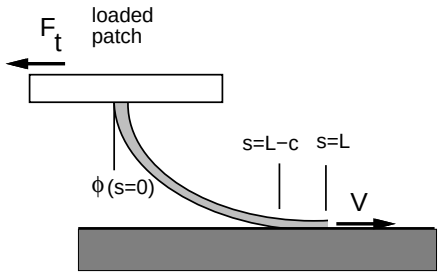

Figure 9. Elastica model of fiber under pure shear loading making side contact with a surface.

centimetre, this corresponds to an average shear force of approximately 210 nN per fiber. This shear force is much higher than predicted by Johnson-Kendall-Roberts (JKR) theory (Johnson *et al.* 1971) for a spherical fiber tip†. For tip contact, the shear force can be estimated from $V_{tip} = \tau A_t$, where A_t is the true tip contact area, and τ is the interfacial shear strength (10 MPa for polypropylene on glass, Pooley & Tabor 1972). (Note that for hard polymers, the true contact area is very small compared to tip size.) The estimated shear force V_{tip} is only 33 nN for tip contact with $r = 0.3 \times 10^{-6}$ m fiber radius, $E = 1$ GPa, and $W_{ad} = 30$ mJ/m^2, the work of adhesion of polypropylene on glass (Gracias & Somorjai 1998).

The tip contact model under estimates the measured shear force by a factor of 6. However, we observe that the measured shear force on the fibers is high enough to cause the initially straight fiber to have *side contact* (figure 9) with the glass. Side contact gives rise to much larger true contact areas than are predicted for

† The Tabor parameter (Johnson 1997) was calculated as 1.6 for a 0.3 μm radius fiber tip. This is closer to the JKR region ($> 3 - 5$) than the DMT region (< 0.1), and hence the JKR model of contact was used.

tip contact. We use a side contact model to provide upper bounds on fiber shear force. Previously, the side contact model was used to explain the normal adhesion of carbon nanotubes, silicon nanowires, and other high-aspect-ratio nanoscale fibers (Majidi *et al.* 2005, Majidi 2007). Specifically, side contact is stable when the surface forces exceed the elastic restoring forces in the deformed fiber. Bending is aided by the shear load V applied to individual fibers as the sample is dragged along a substrate.

To model the large deformations required for side contact, the fibers are treated as elastic rods. In their natural (undeformed) configuration, the fibers are straight. During sliding each fiber is loaded by a shear force $V = V_s$. We let $v = v(s)$ denote the lateral deflection of a fiber of length L caused by a shear load V acting on the tip. The coordinate s represents the arc length from the fiber base. The elastica solution corresponds to the function $\phi = dv/ds$ that satisfies the ordinary differential equation

$$EI\phi'' + V_s \cos\phi = 0\,, \tag{4.1}$$

where the prime denotes the derivative with respect to s, E is elastic modulus, and I is cross sectional moment of inertia.

Letting c denote the length of side contact, it follows that $\phi = \pi/2\,\forall s \in [L-c, L]$. Along the segment $s \in [0, L-c]$, ϕ is the solution to (4.1) along with the boundary conditions $\phi(0) = 0$ and $\phi(L-c) = \pi/2$. The unknown c is determined by the natural boundary condition (Majidi 2007)

$$\frac{1}{2}EI\{\phi'(L-c)\}^2 = \omega\,, \tag{4.2}$$

where ω is the energy of adhesion per unit length of side contact. From Majidi *et*

al. (2005)

$$\omega = 6\left\{\frac{(1-\nu^2)r^2{W_{\rm ad}}^4}{\pi E}\right\}^{1/3}. \tag{4.3}$$

Due to surface roughness of the fiber, the actual energy of adhesion per unit length is likely to be significantly lower than predicted (Persson & Gorb 2003). The length of stable side contact c^* is determined numerically by simultaneously solving equations (4.1), (4.2), for $V = V_m(c)$, where V depends on contact length. The analysis predicts stable side contact under pure shear loading. The length of stable side contact is approximately $c^* = 9.5$ μm.

We consider two bounds for the maximum shear force, spontaneous fracture of the entire interface (V_1) and elastic peeling (V_2). Both bounds will over estimate shear force, as they ignore surface roughness, and possible interference between fibers or backing membrane buckling.

If sliding occurs only after spontaneous fracture of the entire interface, then the strength of the individual fiber contact will be proportional to the total true area of side contact, cb, where

$$b = 8\left\{\frac{(1-\nu^2)r^2W_{\rm ad}}{\pi E}\right\}^{1/3} \tag{4.4}$$

is the width of contact (Majidi *et al.* 2005). For the PP microfiber parameters, $b = 74$ nm. Thus, an upper bound on the shear force for a single fiber in side contact is

$$V_1 = \tau cb. \tag{4.5}$$

From above, the predicted shear force V_1 is 7 μN, greatly exceeding the 210 nN shear force estimated from experiment. (Using 210 nN shear force, the estimated

true contact area per fiber is only 2.1×10^{-10} cm^2, and a cm^2 of patch has estimated true contact area of 0.009 cm^2, only 0.9% of the patch area.)

Contact shear failure can also result from the stretching of the fiber on the surface, which corresponds to the elastic term from the Kendall peel model (Kendall 1975) at low peel angle. Converting from the rectangular strip in the Kendall peel model to a cylinder in side contact, we have:

$$V_2 = \sqrt{2E\pi r^2 \omega}\,. \tag{4.6}$$

The upper bound V_2 for low-angle peeling is 970 nN, again greatly exceeding the average experimental value.

As mentioned above, surface roughness of the fibers will reduce the effective work of adhesion, partially explaining the lower measured shear force. In addition, the estimated side contact length $c^* = 9.5$ μm for an isolated fiber is not likely to be achieved in a structure with average fiber-to-fiber spacing of 1.5 μm. Hence, interactions between neighboring fibers may prevent an average fiber from being in complete side contact.

In contrast to sliding shear force, the tensile pull-off force is quite low, as the fiber will spontaneously transition to tip contact once the shear load is removed. In tip contact, the normal pull-off force $F_{JKR} = \frac{3}{2}\pi r W_{ad} = 42$ nN. In pull-off in the normal direction, height variation of the fibers (approximately uniform distribution, 17-20 μm), combined with low vertical compliance in tension, drastically reduces pull-off force (Majidi *et al.* 2006). In contrast, since side contact length c^* is much greater than height variation, the shear force is much less dependent on fiber height variation. Hence the high shear adhesion and low normal adhesion force is consistent with the side contact elastica model.

(*b*) *Sliding and Viscoelastic Effects*

While the side contact elastica model explains high shear force, it does not directly explain sliding enhanced shear adhesion. Compared to fiber length (20 μm), a long sliding distance (5000 μm) was required to reach maximum shear force (4 N) as shown in figure 3. The long sliding distance required for maximum shear force can be partially explained by a growing estimated contact region being balanced by buckling of the thin polypropylene backing. As shown in image 1 in figure 3, initially only several points are touching the glass, presumably due to natural curvature of the backing and height variation of fibers. As the array slides, a greater number of fibers are engaging and the backing begins buckling. Thus, estimated contact region and buckled area are competing during sliding, which leads to shear force increasing and then saturating.

In our experiments, the natural gecko patch reached maximum shear force after only 200 μm of sliding, with no normal preload. This is comparable to the $\approx$ 100 μm distance seen by Autumn *et al.* (2006b), who used a relatively large normal preload 1 N/cm^2 before sliding, possibly explaining the shorter distance for full fiber engagement. Although we have no direct observations of estimated contact region for the natural gecko patch during sliding, we speculate that buckling may be less significant. This could be due to the gecko lamellar structure, the patch being mounted to a relatively thick (0.02 cm) acetate strip, as well as the relatively small patch size.

Tests with different dragging velocities on the synthetic and natural patches in figure 5 are consistent with shear force increasing with sliding distance, not on sliding velocity, in the range from 48 $\sim$ 240 μm/s. In part II of this paper,

Schubert *et al.* (2007b) test the velocity range from 5 μm/s to 100 μm/s with similar results. We note that the basic shear force model in equations (4.5) and (4.6) has no velocity dependence, although we can not rule out velocity dependent effects at higher velocities.

Relaxation tests support that shear adhesion of microfiber arrays does not depend on an internal viscoelastic property of the material, but rather the surface interactions between PP microfibers and glass. In fact, the shear force drop in figure 3 can be explained by a combination of creep relaxation in the force sensor, and sliding of the fibers under tension after stage motion stopped. The force sensor was directly connected to the stage by a string, and stiffness was measured as 4.5×10^3 N/m. The stage was moved and stopped with the string under tension, and measured force relaxed from 2.79 N to 2.58 N. Sliding of the microfiber patch after stopping the stage was about 150 μm which corresponds to about 0.68 N shear force drop due to sensor and string stiffness. Thus, most of the force drop (about 1 N) in figure 3 can be explained by relaxation (0.21 N) of the force sensor/string combination and sliding (0.68 N) of microfibers.

In contrast, the PSA (0.1 cm^2) did not slide on the glass and shear force increased rapidly while the stage moved, but the PSA relaxed slowly after stopping due to viscoelasticity of the soft polymer. In addition, there was much soft polymer residue on the glass after testing with the PSA, which indicates cohesive failure rather than surface sliding between the PSA and glass. After experiments with the PP microfiber array and natural gecko setal array, no residue was found on the glass. These comparisons support that the viscous deformation typical of detaching PSAs does not seem to occur in the gecko setal array (Gravish *et al.* 2007) or in our

microfiber array. Thus, our microfiber array is free from material degradation as opposed to PSAs which lose viscoelastic energy from internal friction processes such as cavitation and fibrillation (Creton & Fabre 2002). The low viscoelastic losses of the PP GSA are consistent with the observation that the microfiber array has high shear adhesion but has low peel strength, as minimal energy is dissipated during peeling.

(*c*) *Preload independence*

Preload was not an important factor for the saturated shear force as shown in figure 6. As shown in the top left image in figure 3, the initial estimated contact region is very small without sliding displacement, even after application and removal of a compressive preload. After the preload is removed, a small number of fibers in a few regions may be adhering to the glass. Higher and lower preloads do not significantly change initial estimated contact region. We observe that a compressive preload apparently flattens the patch uniformly against the surface, removing any initial curvature. The maximum preload of 0.825 N/cm^2 is less than the load of 1.6 N/cm^2 estimated by Majidi *et al* (2006) to buckle all fibers, hence not all fibers are making contact with the glass during preload. In addition, the image of the estimated contact region shows no evidence of fiber engagement over the whole patch after preload is removed, which is consistent with the non-adhesive default state of the vertical fibers.

A uniformly increasing estimated region of contact during sliding helps to prevent contact concentrations which can lead to the backing buckling. Thus, slight touching the samples with a gloved finger was enough preload for high shear ad-

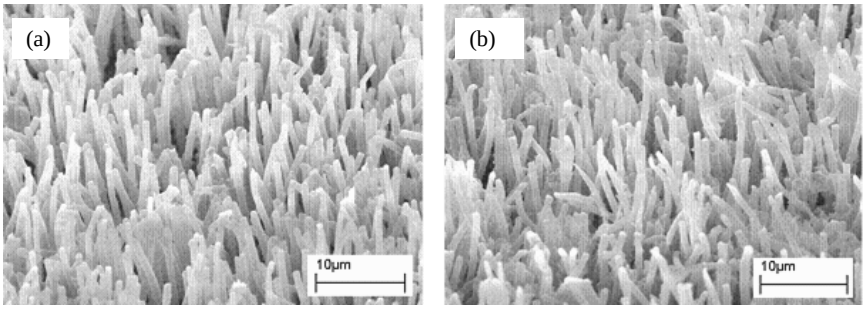

Figure 10. SEM images of microfibers. (a) Before testing. (b) After shearing more than 50 times. The arrow indicates shearing direction. Only a few fibers show deformation. Images in (a) and (b) were taken from different spots.

hesion. We note that the fibers are only stably in side contact with a shear load applied; the normal preload will not engage fibers in side contact, and when preload is removed, fibers will return to the default vertical state. Hence, the independence from compressive preload further supports the side contact model.

(*d*) *Durability*

To examine contamination or wear, we took scanning electron microscope (SEM) images of an unused (see figure 10(a)) and a used sample (see figure 10(b)) which was shear-tested more than 50 times. Contamination or obvious wear was not visible although there are some fibers plastically deformed along the shear direction due to repeated high shear loadings.

Shear adhesion of the samples increased as tests repeated, as shown in figure 8. Enhanced performance is likely caused by angling of the fibers, which makes the fibers more compliant in the normal direction (Sitti & Fearing 2003) and reduces height variation. Examination with an optical microscope showed that microfibers were angled after repeated testings as shown in figure 11. High shear loading an-

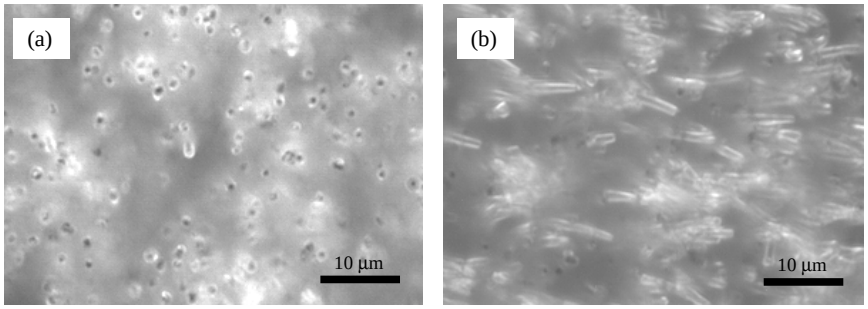

Figure 11. Top view of microfibers through an optical microscope. (a) Vertical fibers. (b) Bent fibers within 10 minutes after loading high shear force. The arrow indicates shearing direction. Images in (a) and (b) were taken from different spots.

gled some of fibers (presumably fibers engaged with surface) but did not angle all fibers uniformly. The angling was not permanent, and fibers recovered to near vertical after several hours when unloaded. Thus, developing a fabrication method for uniformly and permanently angled fibers will be an interesting research topic. Although photolithographic methods have been used to make 25 μm diameter angled fibers (Aksak *et al.* 2007a), the 0.6 μm fiber diameter used here may be a challenge for lithographic methods.

(*e*) *Implications for climbing robots and comparison to other GSAs*

Pure shear tests at the whole-patch scale showed several properties which are important for climbing robots. The peel strength of 0.15 N/m is low enough for easy detachment during vertical running. Shear force increased with sliding distance, which is critical for arresting slip (which could lead to a fall). For both natural and synthetic fiber arrays, shear force recovered after slip events. It is likely that these displacement dependent forces will be important in stabilizing dynamic wall climbers (Autumn *et al.* 2007).

Table 1. *Comparison of other adhesives*

((a) This paper. (b) Santos *et al.* 2007. (c) Gorb *et al.* 2006 and Varenberg & Gorb 2007. (d) Ge *et al.* 2007. (e) Kim & Sitti 2006. (f) Kustandi *et al.* 2007. PP:Polypropylene, PU:Polyurethane, PVS:Polyvinylsiloxane, MWCNT:Multiwalled carbon nanotube.)

	tokay gecko	(a)	(b)	(c)	(d)	(e)	(f)
aspect-ratio	25	30	2.63	2.5	50000	4.4	10
length(μm)/diameter(μm)	100/4	18/0.6	1000/380	100/40	400/0.08	20/4.5	2.5/0.25
material	β-keratin	PP	PU	PVS	MWCNT+PSA	PU	parylene
elastic modulus (GPa)	1.5	1	0.0003	0.003	1000	0.003	2.8
sample area (cm^2)	0.0054	2	4	0.066	0.16	0.03	1
preload pressure(N/cm^2)	< 0.05	< 0.1	0.06	0.2	50	12	1
shear stress (N/cm^2)	55	2	0.3	N.A.	36	N.A.	N.A.
unstructured shear (N/cm^2)	0	~ 0	N.A.	2.27	N.A.	N.A.	N.A.
normal w/o shearing (N/cm^2)	0	~ 0	~ 0	6.06	5	18	0.7

The polypropylene (PP) based microfiber array described in this paper has similar stiffness and aspect ratio to natural tokay gecko. Although actual length ($\sim$ 20 μm) and diameter ($\sim$ 0.6 μm) of the PP fibers are less than those of natural tokay gecko's setae, the unbranched PP fibers have very close dimension to natural anolis (length $\sim$ 12 μm, diameter $\sim$ 0.5 μm) (Ruibal and Ernst 1965). It is expected that the hard material used in the PP microfiber arrays will be important for long term durability and eventual self-cleaning properties which will be difficult with a softer polymer.

It is worthwhile to compare the performance of the PP microfiber array to other recent work in GSAs as summarized in table 1. A particularly important property for a gecko-like adhesive is that one should be able to obtain a high shear force (useful for climbing) yet a low normal force (for easy detach). One can note that a conventional PSA can be used to obtain both high shear adhesion and high normal

pull-off forces on glass. In addition, a low normal preload is desired for ease of engagement during running. Of the GSAs in table 1, only the reported PP fiber array and the soft polyurethane (PU) structures of Santos *et al.* (2007) show the desirable directional adhesive and low preload properties in a macroscale patch. These PU based angled stalks with a sharp tip have negligible normal adhesion without shear load even though the material is soft. It is interesting to note that poly vinyl siloxane (PVS) based mushroom shaped stalks (Gorb *et al.* 2006 and Varenberg & Gorb 2007) have high normal adhesion (6.06 N/cm^2) without shear load but become non-adhesive with shear loading because the mushroom-shaped tips rotate away from the contacting surface.

5. Conclusion

Gecko inspired synthetic microfiber arrays were fabricated with a non-tacky hard polymer. As with natural gecko setal arrays, the fabricated microfiber array shows increasing shear force as a function of sliding distance on smooth glass. This unique property provides stability of the detachable adhesive (robust to a shear disturbance or vibration). Comparisons with PSA supports that shear force from the microfiber array does not depend on viscous creep, thus, low energy detachment is possible. The durable microfiber array was able to hold as great as 4 N in shear with a 2 cm^2 nominal patch area when the array slid 1 cm and had shear stress greater than 9 N/cm^2 for the estimated contact region, approximately 15% of the natural gecko lamella patch we tested. The high shear adhesion force is due to side contact, which could substitute for complicated spatula structures on smooth surfaces. The PP microfiber array has sufficient shear adhesion for small climbing robots, and

has the unique property that performance improves with use, likely due to fiber deformation.

This work was supported by NSF NIRT (No. EEC-034730). The authors wish to thank S. Baek for helping with the macro-scale force sensor, B. Bush for SEM work, Prof. Autumn's lab for providing natural gecko setal arrays and E. Steltz, A. Hoover, N. Gravish, and S. Baek for helpful comments.

References

Aksak, B., Murphy, M. P. & Sitti, M. 2007a Adhesion of biologically inspired vertical and angled polymer microfiber arrays. *Langmuir* **23**, 3323-3332.

Aksak, B. Sitti, M., Casell, A., Li,J., Meyyappan,M., & Callen,P. 2007b Friction of partially embedded vertically aligned carbon nanofibers inside elastomers, *Appl. Phys. Lett.* **91**, no. 061906, 2007.

Antoniou, A. & Bastawros, A.F. 2003 Deformation characteristics of tin-based solder joints. *J. Mater. Res.* **18**, 2304-2310.

Autumn, K. 2007 Gecko adhesion: structure, function, and applications. *MRS Bull.* **32** 473-478.

Autumn, K. & Gravish, N. 2007 (in press) Gecko adhesion: evolutionary nanotechnology. *Philos. Trans. R. Soc. A-Math. Phys. Eng. Sci.*.

Autumn, K., Hsieh, S.T., Dudek, D.M., Chen, J., Chitaphan, C. & Full, R.J. 2007 Dynamics of geckos running vertically, *J. Exp. Biol.* **209**, 206-272.

Autumn, K., Liang, Y. A., Hsieh, S. T., Zesch, W., Chan, W.-P., Kenny, W. T., Fearing, R. & Full, R. J. 2000 Adhesive force of a single gecko foot-hair. *Nature* **405**, 681.685. **doi:10.1038/35015073**

Autumn, K., Majidi, C., Groff, R. E., Dittmore, A. & Fearing, R. S. 2006a Effective elastic modulus of isolated gecko setal arrays. *J. Exp. Biol.* **209**, 3558-3568.

Autumn, K., Dittmore A., Santos, D., Spenko, M. & Cutkosky, M. 2006b Frictional adhesion: a new angle on gecko attachment. *J. Exp. Biol.* **209**, 3569-3579.

Autumn, K. & Hansen, W. 2006c Ultrahydrophobicity indicates a non-adhesive default state in gecko setae *J. Comp. Physiol. A* **192** 1205. **doi:10.1007/s00359-006-0149-y**

Creton, C. & Fabre, P. 2002 *In Adhesion science and engineering: vol. I - the mechanics of adhesion* (ed. A. V. Pocius, D. A. Dillard, & M. Chaudhury), Tack, pp. 535-576. Amsterdam, The Netherlands: Elsevier.

Ge, L., Sethi, S., Ci L., Ajayan, P. M. & Dhinojwala, A. 2007 Carbon nanotube-based synthetic gecko tapes. *Proc. Natl. Acad. Sci. U. S. A.* **104**, 10792.10795.

Geim, A. K., Dubonos, S. V., Grigorieva, I. V., Novoselov, K. S., Zhukov, A. A. & Shapoval, S. Yu. 2003 Microfabricated adhesive mimicking gecko foot-hair. *Nat. Mater.* **2**, 461-463.

Gorb, S., Varenberg, M., Peressadko, A. & Tuma, J. 2006 Biomimetic mushroom-shaped fibrillar adhesive microstructure, *J. R. Soc. Interface* **4** 271-275. **doi:10.1098/rsif.2006.0164**

Gracias, D. H. & Somorjai, G. A. 1998 Continuum force microscopy study of the elastic Modulus, hardness and friction of polyethylene and polypropylene surfaces. *Macromolecules* **31**, 1269-1276.

Gravish, N., Wilkinson, M. & Autumn, K. 2007 Frictional and elastic energy in gecko adhesive attachment. *J. R. Soc. Interface* **doi:10.1098/rsif.2007.1077**.

Johnson, K. L., Kendall, K. & Roberts, A. D. 1971 Surface energy and the contact of elastic solids. *Proc. R. Soc. Lond. A* **324** 301-313.

Johnson, K.L. 1997 Adhesion and friction between a smooth elastic spherical asperity and a plane surface, *Proc. R. Soc. Lond. A* **453** 163-179.

Kendall, K. 1975 Thin-film peeling — the elastic term. *J. Phys. D. Appl. Phys.* **8** 1449-1452.

Kim, S. & Sitti, M. 2006 Biologically inspired polymer microfibers with spatulate tips as repeatable fibrillar adhesives. *Appl. Phys. Lett.* **89** 261911.

Kustandi, T.S., Samper, V.D., Yi, D.K., Ng, W.S., Neuzil, P. & Sun, W. 2007 Self-assembled nanoparticles based fabrication of gecko foot-hair-inspired polymer nanofibers, *Adv. Funct. Mater.* **17** 2211-2218.

Majidi, C. 2007 Remarks on formulating an adhesion problem using Euler's elastica. *Mech. Res. Commun.* **34**, 85-90.

Majidi, C., Groff, R. E., Maeno, Y., Schubert, B., Baek, S., Bush, B., Maboudian, R., Gravish, N., Wilkinson, M., Autumn, K. & Fearing, R. S. 2006 High friction from a stiff polymer using micro-fiber arrays. *Phys. Rev. Lett.* **97**, 076103.

Majidi, C., Groff, R. E. & Fearing, R. S. 2005 Attachment of fiber array adhesive through side contact. *J. Appl. Phys.* **98**, 103521.

Peattie, A. M., Majidi, C., Corder, A. & Full, R. J. 2007 Ancestrally high elastic modulus of gecko setal β-keratin *J. R. Soc. Interface* **doi:10.1098/rsif.2007.0226**.

Persson, B.N.J. & Gorb, S. 2003 The effect of surface roughness on the adhesion of elastic plates with applications to biological systems. *J. Chem. Phys.* **119** 11437-11444.

Pooley, C. M. & Tabor, D. 1972 Friction and Molecular Structure: The Behaviour of Some Thermoplastics. *Proc. R. Soc. Lond. A* **329**, 251-274.

Ruibal, R. & Ernst, V. 1965 The structure of the digital setae of lizards, *J. Morph.* **117** 271-294.

Santos, D., Kim, S., Spenko, M., Parness, A. & Cutkosky, M. 2007, Directional adhesive structures for controlled climbing on smooth vertical surfaces. In *Proc. IEEE ICRA*, 1262-1267.

Schubert, B., Majidi, C., Groff, S., Baek, S., Bush, B., Maboudian, R. & Fearing, R.S. 2007a, Towards friction and adhesion from high modulus microfiber arrays. *J. Adhesion Sci. Tech.* **21** 1297-1315.

Schubert, B., Lee, J., Majidi, C., & Fearing, R.S. 2007b, Sliding induced adhesion of stiff polymer microfiber arrays: 2. Microscale contact behaviour, submitted to *J. R. Soc. Interface* Nov. 2007.

Sitti, M. & Fearing, R. S. 2003 Synthetic gecko foot-hair micro/nano-structures as dry adhesives. *J. Adhesion Sci. Tech.* **18**, 1055-1074.

Varenberg, M. & Gorb, S. 2007 Shearing of fibrillar adhesive microstructure: friction and shear-related changes in pull-off force, *J. R. Soc. Interface* **4** 721-725. **doi:10.1098/rsif.2007.0222**

Zhao, Y., Tong, T., Delzeit, L., Kashani, A., Meyyappan, M. & Majumdar, A. 2006 Interfacial energy and strength of multiwalled-carbon-nanotube-based dry adhesive. *J. Vac. Sci. Tech. B* **24** 331-335.